PNAS
www.pnas.org

Supplementary Information for

Silent polio outbreak in Rahat, Israel: Epidemiologic findings based on modeling of environmental surveillance data

A.F. Brouwer, J.N.S. Eisenberg, C.D. Pomeroy, L.M. Shulman, M. Hindiyeh, Y. Manor, I. Grotto, J.S. Koopman, M.C. Eisenberg

Corresponding Authors: M.C. Eisenberg, J.N.S. Eisenberg.
E-mail: marisae@umich.edu, jnse@umich.edu

This PDF file includes:

Supplementary text
Figs. S1 to S7
Table S1
Captions for Databases S1 to S4
References for SI reference citations

Other supplementary materials for this manuscript include the following:

Databases S1 to S4

www.pnas.org/cgi/doi/10.1073/pnas.1808798115

Supporting Information Text

SEIR model with environmental surveillance. Our baseline model is an ordinary differential equation (ODE) SEIR model with environmental surveillance (Eq. (1)). The model considers fractions of susceptible (S), exposed (or, more accurately, latently infected) (E), infectious (I), and recovered (R) individuals, as well as the concentration of polio in sewage (W). Infection is assumed to be directly transmitted from infectious individuals to susceptible individuals (at rate β). Once infected, latent individuals become infectious at rate σ, and infectious individuals recover at rate γ. Infectious individuals shed into sewage at rate α, and pathogens die-off at rate ξ. A model diagram is given in Figure S1.

$$\begin{aligned} \dot{S} &= -\beta SI, \\ \dot{E} &= \beta SI - \sigma E, \\ \dot{I} &= \sigma E - \gamma I, \\ \dot{W} &= \alpha I - \xi W. \end{aligned} \qquad [1]$$

Although this model is inspired by other models with environmental compartments, such as the SIWR (1, 2) and EITS (3, 4) models, it is not a model of environmentally mediated transmission, i.e., we assume that there is no transmission resulting from ingestion of pathogens from the the environment (in this case, sewage), although transmission may occur person-to-person via either oral-oral or fecal-oral tranmsission (these are not distinguished in our model). The W compartment solely represents a reservoir for environmental surveillance. If the environmental surveillance is analyzed by qPCR, with the following measurement equation,

$$y = \frac{\ln(\tau/W)}{\ln 2} = \log_2(\tau/W), \qquad [2]$$

the sample concentration W (Eq. (2)) corresponds to the concentration of model compartment W (Eq. (1)) when concentration is given in copy numbers per qPCR sample volume.

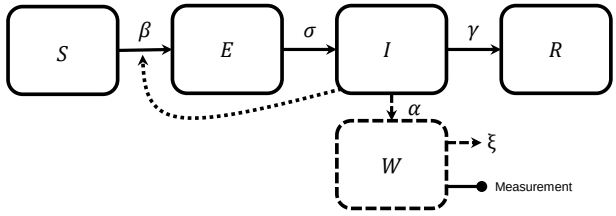

Fig. S1. Schematic of an SEIR model with sewage data.

Overview of identifiabiltiy and model reparameterization. Because the use of PCR CT data is novel in the context of fitting to disease transmission models, we must clearly understand what parametric information is available in the data for the model.

Heuristically, the environmental surveillance data can give us the shape of the epidemic. Because epidemic shape is controlled by the basic reproduction number and the basic reproduction number controls the epidemic final size, we can determine the appropriate scaling to convert the environmental data into disease incidence.

More formally, the following proposition gives the results of structural identifiability analysis for the SEIR model with environmental surveillance (Eq. (1), Figure S1).

Proposition 1. *Given perfectly measured PCR CT data y (Eq. (2)), the SEIR model with environmental surveillance (Eq. (1)) has four identifiable parameter combinations: $\beta\tau/\alpha$, $\gamma+\sigma$, $\gamma\sigma$, and ξ. Here, γ and σ locally identifiable, here meaning that each can only take one of two values and knowing one (or even which is larger) resolves the other. If σ is known or identifiable and $R(0) = 0$, then β, $S(0)$, $E(0)$, and $I(0)$ are identifiable and S, E, I, and R are observable. After a non-dimensionalizing scaling, $\bar{W} = \xi W/\alpha$, $\bar{W}(0)$ is identifiable and $\bar{W}$ is observable. The model reparameterized with this scaling is locally identifiable.*

The proof of this statement, with additional discussion and details, is provided in the next section. This theorem demonstrates that our sewage equations need to be rescaled to be observable (although other rescalings are legitimate, we use the non-dimensionalizing one suggest by Tien and Earn (1)). Because of the unknown parameters α and τ, we cannot directly observe W, the concentration of poliovirus in the sewage. A given CT value could have arisen from a higher poliovirus concentration (related to α) and higher threshold τ, or lower values of both, as long the proportion was the same. After this rescaling, we have

$$\dot{\bar{W}} = \xi(I - \bar{W}), \qquad [3]$$

for the SEIR with environmental surveillance model. The measurement equation is rescaled as well,

$$y = \log_2((\xi\tau/\alpha)/\bar{W}). \qquad [4]$$

Using the same method as in the proof of Proposition 1, we can analyze the identifiability of the full Israel outbreak model. Under the same assumptions, τ/α_o, τ/α_w, β, ρ, γ, σ, and ξ are theoretically identifiable.

Whether each of these parameters or parameter combinations are practically identifiable given the actual data is another consideration. In particular, in many cases, the pathogen decay rate ξ, although structurally identifiable, will not be practically identifiable (2, 5). Here, the pathogen decay rate can be arbitrarily large and not significantly change the likelihood (see section *The practical unidentifiability of the pathogen decay rate*, Figure S2). Because this parameter unidentifiability can cause instability in optimization algorithms, we would like to remove it from the model by reparameterization. However, because the unidentifiability is practical rather than structural, no algebraic reparameterization exists. Nonetheless, we observe that an arbitrarily large pathogen decay means that $\dot{\bar{W}}$ can be arbitrarily large and that, consequently, $\bar{W}$ closely follows the values of I. Hence, this practical unidentifiability of the pathogen decay rate is really a statement that

$$\bar{W} \approx I. \tag{5}$$

In truth, we expect the pathogen decay rate to be on lower end of its likelihood-based confidence interval. In the absence of experimental estimates for the decay rate, though, employing this approximation in Eq. (5) allows us to fit a practically identifiable model and successfully estimate the remaining parameters (see profile likelihoods for all other estimated parameters in *Profile likelihoods*). Hence, one can use the measurement equation

$$y = \log_2((\xi\tau/\alpha)/I). \tag{6}$$

Even when ξ is not practically identifiable, the parameter combination $\xi\tau/\alpha$ may be.

The OPV1-to-WPV1 transmission rate ratio ρ, while structurally identifiable, is also not practically identifiable. We have, therefore, fixed it to a reasonable value from the literature. This practical unidentifiability occurs because the transmission of OPV1 is on the same timescale as vaccination (the basic reproduction number for OPV1 is less than one here), and so there is no dynamic information to distinguish between OPV1 acquired through vaccination versus transmission in the environmental surveillance data. This practical unidentifiability is important to consider whenever one models multiple modes of transmission or multiple subpopulations that are measured from the same environmental pool.

Structural identifiability. We use the differential algebra approach to structural identifiability, more details of which may be found elsewhere (6–8). Briefly, the differential algebra approach seeks to construct a set of input–output equations, that is, monic, polynomial equations that are functions of the observed quantities and their derivatives and that are an equivalent to the original differential equations. The parameter combinations that are the coefficients of the input–output equations contain all parameteric information available in the model output trajectories, so the model is identifiable if and only if there is a one-to-one map from the model parameters to the input–output equation coefficients.

Here, we provide a detailed example of the differential algebra approach to structural identifiability for an SEIR model with PCR CT sewage data. The measurement equation is $y = \ln(\tau/W)/\ln 2$. Then, y contains equivalent information to $v = W/\tau$, which is a more convenient measurement to work with. Our model and measurement equations are

$$\dot{S} = -\beta SI, \tag{7}$$
$$\dot{E} = \beta SI - \sigma E, \tag{8}$$
$$\dot{I} = \sigma E - \gamma I, \tag{9}$$
$$\dot{W} = \alpha I - \xi W, \tag{10}$$
$$v = W/\tau. \tag{11}$$

Proof. The goal is to find an input–output equation for this model, i.e., a monic polynomial in terms of v, derivatives of v, and the model parameters that has the same observed dynamics as the original system of equations.

First, we substitute $W = \tau v$ into Eq. (10) and simplify.

$$\tau\dot{v} = \alpha I - \xi\tau v. \tag{12}$$

We then solve for I and substitute

$$I = \frac{\tau}{\alpha}(\dot{v} + \xi v) \tag{13}$$

into the first three equations,

$$\dot{S} = -\beta S\left(\frac{\tau}{\alpha}(\dot{v} + \xi v)\right), \tag{14}$$
$$\dot{E} = \beta S\left(\frac{\tau}{\alpha}(\dot{v} + \xi v)\right) - \sigma E \tag{15}$$
$$\frac{\tau}{\alpha}(\ddot{v} + \xi\dot{v}) = \sigma E - \frac{\gamma\tau}{\alpha}(\dot{v} + \xi v). \tag{16}$$

We then solve for E in terms of v and its derivatives,

$$E = \frac{\tau}{\sigma\alpha}\left(\ddot{v} + (\xi + \gamma)\dot{v} + \gamma\xi v\right), \tag{17}$$

and plug it into Eq. (15), simplifying to

$$v^{(3)} + (\xi+\gamma+\sigma)\ddot{v} + (\gamma\xi+\sigma\xi+\sigma\gamma)\dot{v} + (\sigma\gamma\xi)v = \sigma\beta S(\dot{v}+\xi v). \tag{18}$$

We solve for S

$$S = \frac{v^{(3)} + (\xi+\gamma+\sigma)\ddot{v} + (\gamma\xi+\sigma\xi+\sigma\gamma)\dot{v} + (\sigma\gamma\xi)v}{\sigma\beta(\dot{v}+\xi v)}, \tag{19}$$

and plug this expression into Eq. (14), simplifying to

$$\begin{aligned}
0 = {} & v^{(4)}\dot{v} + \xi v^{(4)} v - v^{(3)}\ddot{v} + (\beta\tau/\alpha)v^{(3)}\dot{v}^2 \\
& + 2\xi(\beta\tau/\alpha)v^{(3)}\dot{v}v + (\gamma+\sigma)v^{(3)}\dot{v} \\
& + \xi^2(\beta\tau/\alpha)v^{(3)}v^2 + \xi\left((\gamma+\sigma)+\xi\right)v^{(3)}v \\
& - \left((\gamma+\sigma)+\xi\right)(\ddot{v})^2 + (\beta\tau/\alpha)\left((\gamma+\sigma)+\xi\right)\ddot{v}\dot{v}^2 \\
& + 2\xi(\beta\tau/\alpha)\left((\gamma+\sigma)+\xi\right)\ddot{v}\dot{v}v \\
& - \xi\left((\gamma+\sigma)+\xi\right)\ddot{v}\dot{v} + \xi^2(\beta\tau/\alpha)\left((\gamma+\sigma)+\xi\right)\ddot{v}v^2 \\
& + \xi^2\left(\gamma+\sigma\right)\ddot{v}v + (\beta\tau/\alpha)\left(\xi(\gamma+\sigma)+\gamma\sigma\right)\dot{v}^3 \\
& + \xi(\beta\tau/\alpha)\left(\left(\xi(\gamma+\sigma)+2\gamma\sigma\right)\dot{v}^2 v - \xi^2\left(\gamma+\sigma\right)\dot{v}^2\right. \\
& + \xi^2(\beta\tau/\alpha)\left(\xi(\gamma+\sigma)+3\gamma\sigma\right)\dot{v}v^2 + \xi^3\gamma\sigma(\beta\tau/\alpha)v^3.
\end{aligned} \tag{20}$$

This equation is a monic polynomial of v and its derivatives that describes the same dynamics as the original set of differential equations; hence, it is an input–output equation for our system. The coefficients of this input–output equation contain all of the parametric information available from observing trajectories of v. From these coefficients, we can write a reduced set of identifiable parameter combinations $\{\beta\tau/\alpha, \gamma+\sigma, \gamma\sigma, \xi\}$.

Because we know both $\gamma+\sigma$ and $\gamma\sigma$, there are only two solutions for the values of γ and σ, and we say that they are locally identifiable. This locally identifiability is characteristic of SEIR models and is typically easily resolved in practice.

Now, generically, we have $S+E+I+R=1$, but, if our target population is designated in such a way that $R(0)=0$, then we can separate β from its identifiable combination as follows. Note that

$$\begin{aligned}
1 = {} & S(0) + I(0) + E(0) \\
= {} & \frac{v^{(3)}(0) + (\xi+\gamma+\sigma)\ddot{v}(0) + (\gamma\xi+\sigma\xi+\sigma\gamma)\dot{v}(0) + (\sigma\gamma\xi)v(0)}{\sigma\beta(\dot{v}(0)+\xi v(0))} \\
& + \frac{\tau}{\alpha}(\dot{v}(0)+\xi v(0)) + \frac{\tau}{\sigma\alpha}\left(\ddot{v(0)} + (\xi+\gamma)\dot{v(0)} + \gamma\xi v(0)\right).
\end{aligned} \tag{21}$$

This expression can be simplified to

$$\begin{aligned}
0 = {} & v^{(3)}(0) + (\beta\tau/\alpha)\ddot{v}(0)\dot{v}(0) + (\beta\tau/\alpha)\xi\ddot{v}(0)v(0) \\
& + (\gamma+\xi+\sigma)\ddot{v}(0) + (\beta\tau/\alpha)(\gamma+\xi+\sigma)\dot{v}(0)^2 \\
& + \xi(\beta\tau/\alpha)(2(\gamma+\sigma)+\xi)\dot{v}(0)v(0) \\
& + (\xi(\gamma+\sigma)+\gamma\sigma-\sigma\beta)\dot{v}(0) \\
& + \xi^2(\beta\tau/\alpha)(\gamma+\sigma)v(0)^2 + (\xi\sigma\gamma-\xi\sigma\beta)v(0).
\end{aligned} \tag{22}$$

Rearranging, we see that $\sigma\beta$ is equal to a known quantity. If σ is known or is otherwise resolved from γ, then β is identifiable.

Now, we notice that W is not observable from v because τ is not identifiable. Thus, we introduce the scaling

$$\bar{W} = \xi W/\alpha, \tag{23}$$

so that

$$\dot{\bar{W}} = \xi(I-\bar{W}). \tag{24}$$

Although only scaling by α is needed to achieve observability, scaling by ξ, too, is convenient in that it non-dimensionalizes the compartment.

Under these assumptions (i.e., that σ is known and $R(0)=0$), the initial conditions $\bar{W}(0)$, $S(0)$, $I(0)$, and $E(0)$ are identifiable. Hence, $\bar{W}$, S, E, I, and R are observable. □

Practical identifiability. We use a numerical, profile likelihood approach to assess practical identifiability and do parameter estimation (9, 10). Briefly, we calculate the the minimum negative log-likelihood at a series of values of one parameter while fitting the other parameters. The resulting parameter profile is the curve of the negative log-likelihood as a function of the profiled parameter p_i. The parameter profile will achieve its minimum at the maximum likelihood value, $\hat{p}_i$. If the profile is flat, the parameter cannot be uniquely determined by the data and is unidentifiable. If the profile has strong curvature, the parameter is identifiable. The curve may also be have shallow curvature, or be flat on one side, in which case the parameter is said to be practically unidentifiable.

Confidence intervals are determined by setting an appropriate likelihood threshold value, dependent on the level of significance, and defining the confidence interval as all values of p_i for which the profile likelihood value is less than the threshold. The threshold for log-likelihood-based simultaneous confidence intervals is given by $\chi^2(1-\alpha, \mathrm{df})/2$, where $\chi^2(1-\alpha, \mathrm{df})$ is the chi-square distribution with level of significance equal to α and degrees of freedom equal to the number of parameters (9).

The practical unidentifiability of pathogen decay rate. Often, the environmental data for infectious disease models with an environmental compartment is not sufficient to uniquely determine the pathogen decay rate, ξ, even when it is a theoretically identifiable parameter (2, 5). Typically, the pathogen decay rate can be arbitrarily large and still fit the data well. As seen in Figure S2, likelihood flattens as $\xi \to \infty$. In this case, ξ does have a local minimum around 1, but it does not achieve statistical significance under the assumed error structure.

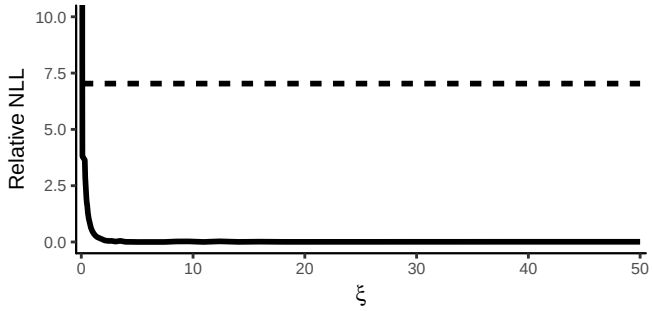

Fig. S2. Profile likelihood of the pathogen decay rate ξ with a 95% simultaneous confidence interval threshold for parameter estimation on six parameters.

Profile likelihoods. Profile likelihoods for fitted parameters and initial conditions are shown in Figure Eq. (S3) with 95% confidence intervals thresholds. All parameters are practically identifiable because the likelihood-based confidence intervals are finite. The shape of the profile likelihood for $\xi\tau/\alpha_w$ is interesting. As the parameter decreases, the $\mathcal{R}_0$ of the corresponding parameters decreases toward 1, indicating that there are a range of plausible trajectories through the data, from broad, flat peaks to faster epidemics with more pronounced turn-overs.

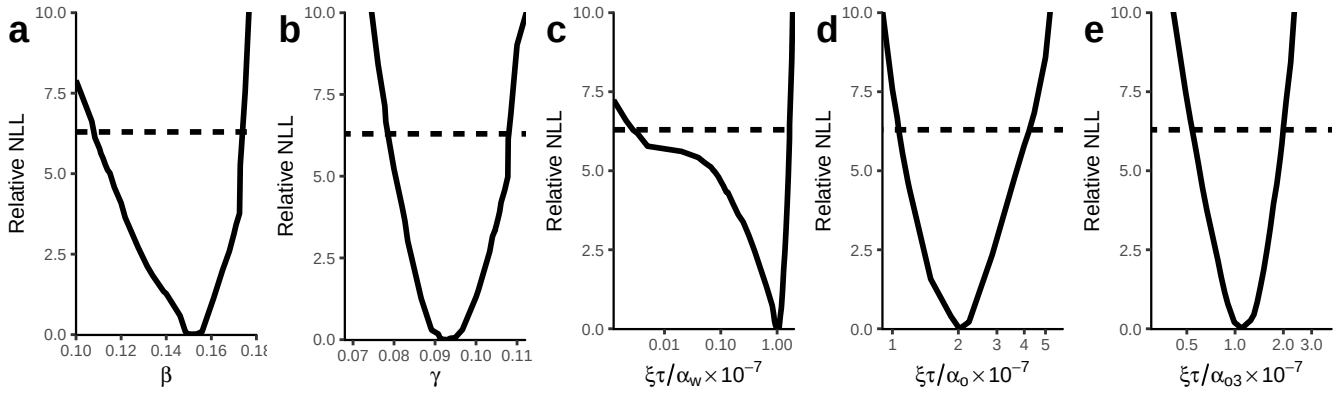

Fig. S3. Profile likelihood plots of the fit parameters (a. β, b. γ, c. $\xi\tau/\alpha_w$, d. $\xi\tau/\alpha_o$, e. $\xi\tau/\alpha_{o3}$). The black line is the profile likelihood, and the dotted line is the threshold value for 95% simultaneous confidence intervals for parameter estimation on four parameters. All parameters are practically identifiable because of the finite likelihood-based confidence intervals.

OPV3 modeling and results. We model OPV3 analogously to OPV1. We assume OPV3 has the same latent and infectious period as WPV1 and OPV1 (11), but we fix the transmission reduction parameter θ_3 to 0.8×0.25=0.2, to reflect the transmission ratio of 0.8 between WPV3 and WPV1 and the ratio of 0.25 between OPV3 and WPV3 (11). We allow the shedding parameter α_{o3} to differ from α_o or α_w. We define E^v_{o3}, E^t_{o3}, I^v_{o3}, I^t_{o3}, R^t_{o3}, and $R^v{}_0o3$ analogously to the variables for OPV1; S_{o3} is defined as all individuals who are susceptible to OPV3. We do not track the joint infection status of OPV1 and OPV3. Since, either WPV1 nor OPV1 confer protection against OPV3, a person could simultaneously be in, for example, I^t_o and S_{o3}. The equations governing the OPV3 infection states are

$$\begin{aligned}
\dot{S}_{o3} &= -\beta\theta_3 S_{o3}(I^t_{o3} + I^v_{o3}) + \varphi S_{o3}, \\
\dot{E}^v_{o3} &= \varphi S_{o3} - \sigma E^v_{o3}, \\
\dot{E}^t_{o3} &= \beta\theta_3 S_{o3}(I^t_{o3} + I^v_{o3}) - \sigma E^t_{o3}, \\
\dot{I}^v_{o3} &= \sigma E^v_{o3} - \gamma I^v_{o3}, \qquad \dot{R}^v_{o3} = \gamma I^v_{o3}, \\
\dot{I}^t_{o3} &= \sigma E^t_{o3} - \gamma I_{o3}, \qquad \dot{R}^t_{o3} = \gamma I^t_{o3}.
\end{aligned} \tag{25}$$

Then, the equations for the concentration and scaled concentration of OPV3 in sewage are

$$\begin{aligned}
\dot{W}_{o3} &= \alpha_{o3}(I^v_{o3} + I^t_{o3}) - \xi W_{o3}, \\
\dot{\bar{W}}_{o3} &= \xi(I^v_{o3} + I^t_{o3} - \bar{W}_{o3}).
\end{aligned} \tag{26}$$

As before, we make the approximation $\xi \to \infty$ and use the measurement equation

$$y_{o3} = \log_2((\xi\tau/\alpha_{o3})/(I^v_{o3} + I^t_{o3})). \tag{27}$$

In Figure S4, we plot the model fit to the OPV3 PCR CT data. We estimate $\xi\tau/\alpha_{o3}$ to be 1.09×10^7 (95%CI: 0.5–2.0×10^7).

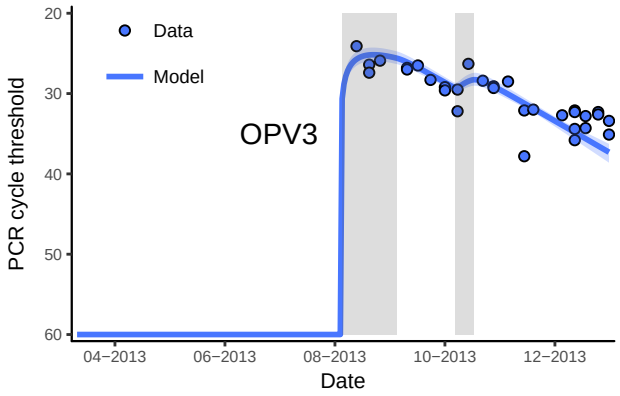

Fig. S4. PCR cycle threshold (CT) data and model fits for OPV3 in sewage. The PCR detection limit corresponds corresponds to about a CT of 40, and experiments were run to 60. The ribbons give the confidence intervals for the maximum likelihood trajectory using likelihood-based estimates of the 95% confidence parameter region. The gray bars give the time periods of the approximate bOPV campaigns.

Fraction-scale plots. In Figure 2, we plotted the fit to the environmental surveillance data on the CT scale, i.e., on a log-scale. Here, for completeness, we include the same plots on the linear scale (Figure S5).

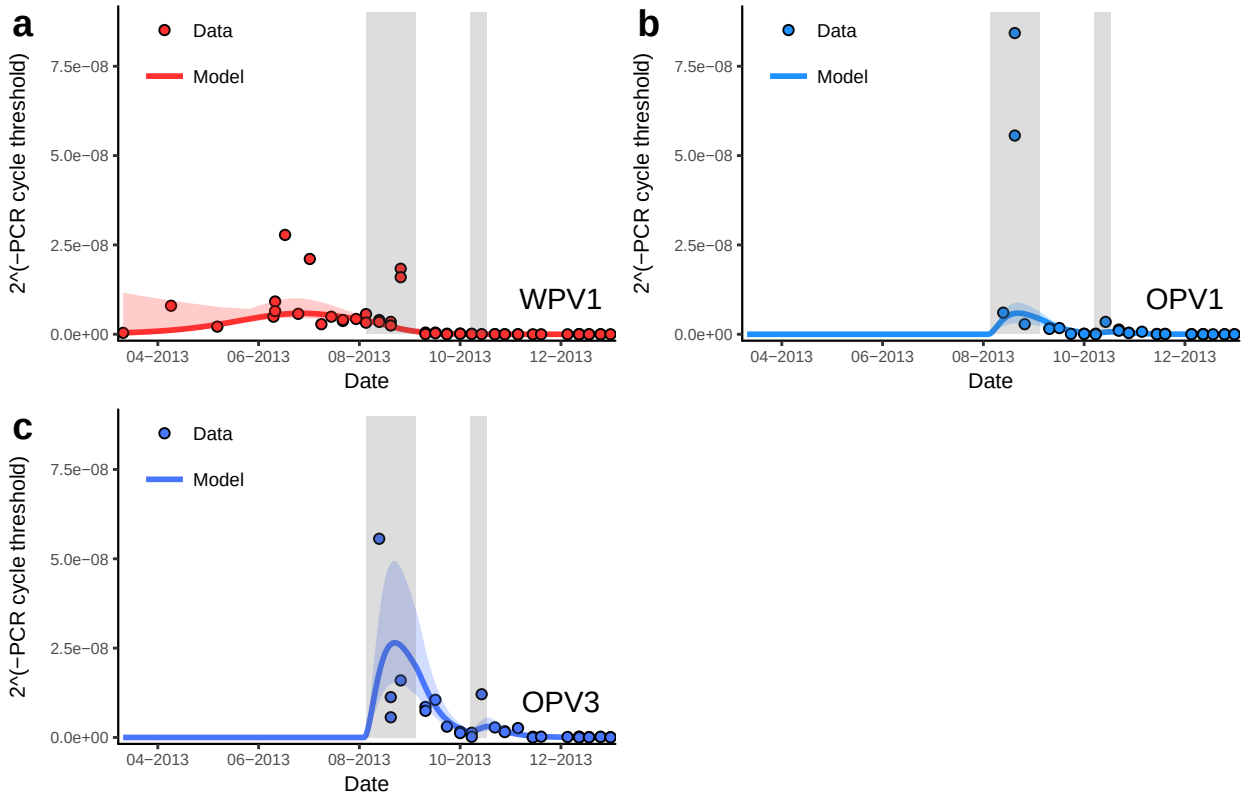

Fig. S5. PCR cycle threshold data and model fits for (a) WPV1, (b) OPV1, (c) OPV3 strains in sewage on the linear (non-log) scale. The gray bars give the time periods of the modeled active bOPV campaign.

Stool sample plots. The stool sample data, weighted weekly moving average, and Clopper–Pearson confidence intervals and with a weighted weekly moving average are presented here on a scale that demonstrates the full uncertainty.

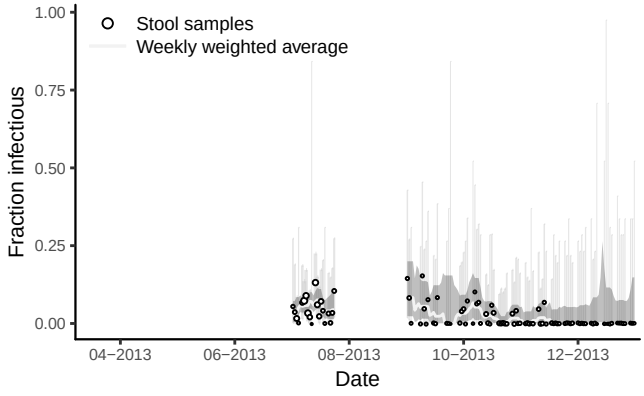

Fig. S6. Prevalence of WPV1 in stool of a convenience sample of under-8 year olds in Southern Israel, where point size is scaled to sample size, with weekly weighted moving average and 95% Clopper–Pearson confidence intervals for the data points and the weekly average.

Transmission with seasonal variation. In the pre-vaccination era, cases of polio were strongly seasonal in temperate areas; the cause of this seasonality is unknown, but may be related to temperature or humidity (12). The average monthly high temperature in this region of Israel ranges from 62°F in January to 92°F in July, while the the relative humidity ranges from 35% in May to 50% in January (Figure S7) (13). It is unclear whether these climatic variations would substantially impact poliovirus transmission. Following Yaari et al. (14), we modeled seasonal variation in transmission with a periodic function; here we use a sinusoidal function,

$$\beta(t) = \beta_0 \cdot \left(1 + \psi \cdot \cos\left(\frac{2\pi}{365}(t - \omega)\right)\right) \quad [28]$$

The best fit model with seasonal variation estimated relatively little amplitude of transmission variation (Figure S7a). Moreover, the phase of the periodic function is not identifiable (that is, a model with any given phase could fit the data within the likelihood threshold). The best fit model is shown in Figure S7b and c and Table S1. Including seasonal variation did not significantly improve model fit by an AIC criterion. Hence, we did not include seasonal variation in our final analysis.

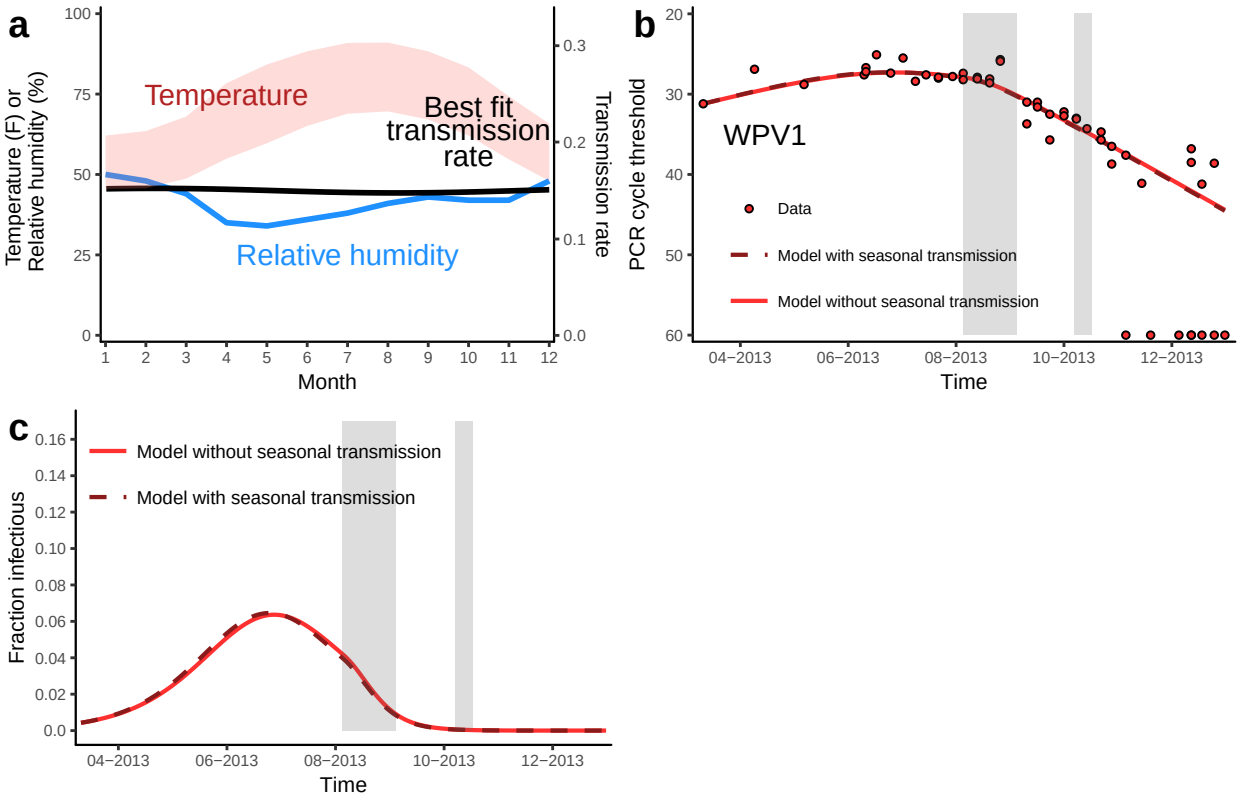

Fig. S7. Monthly average low and high temperature (red) and relative humidity (blue) in Beer Sheva, a city near Rahat in the Negev region of Israel (13). The best-fit sinusoidal seasonal transmission rate is given in black. b) PCR cycle threshold data and model fits for WPV1 for the models with and without a seasonal transmission rate. c) Best-fit epidemic trajectories for the models with and without a seasonal transmission rate.

Table S1. Estimated model parameter values for the model with seasonal transmission rate (with 95% Wald confidence intervals).

Parameter	Value	95% C.I.
Average WPV1 transmission rate, β_0	0.150/d	(0.145, 0.155)
Day of peak transmission, ω	Mar. 9	*
Deviation from average transmission, ψ	1.5×10^{-2}	*
Recovery rate, γ	0.092/d	(0.089, 0.095)
OPV1 sewage scaling parameter, $\xi\tau/\alpha_o$	2.05E7	(1.5E7, 2.8E7)
WPV1 sewage scaling parameter, $\xi\tau/\alpha_w$	1.05E7	(1.0E6, 1.1E6)

*:These parameters are not practically identifiable.

Additional data table S1 (poliodata_WPV1.csv)
Quantiatitive PCR cycle threshold data for wild poliovirus type 1 in the Rahat sewage treatment plant in 2013.

Additional data table S2 (poliodata_OPV1.csv)
Quantiatitive PCR cycle threshold data for vaccine poliovirus type 1 in the Rahat sewage treatment plant in 2013.

Additional data table S3 (poliodata_OPV3.csv)
Quantiatitive PCR cycle threshold data for vaccine poliovirus type 3 in the Rahat sewage treatment plant in 2013.

Additional data table S4 (stool_samples_WPV1.csv)
Stool sample survey data.

References

1. Tien JH, Earn DJD (2010) Multiple transmission pathways and disease dynamics in a waterborne pathogen model. *Bulletin of Mathematical Biology* 72(6):1506–33.
2. Eisenberg MC, Robertson SL, Tien JH (2013) Identifiability and estimation of multiple transmission pathways in cholera and waterborne disease. *Journal of Theoretical Biology* 324:84–102.
3. Li S, Spicknall IH, Koopman JS, Eisenberg JNS (2009) Dynamics and control of infections transmitted from person to person through the environment. *American Journal of Epidemiology* 170(2):257–265.
4. Brouwer AF, et al. (2017) Dose-response relationships for environmentally mediated infectious disease transmission models. *PLOS Computational Biology* 13(4):e1005481.
5. Lee EC, et al. (2017) Model distinguishability and inference robustness in mechanisms of cholera transmission and loss of immunity. *Journal of Theoretical Biology* 420:68–81.
6. Saccomani M, Audoly S, Bellu G, D'Angio L (2001) A new differential algebra algorithm to test identifiability of nonlinear systems with given initial conditions in *Proceedings of the 40th IEEE Conference on Decision and Control (Cat. No.01CH37228)*. (IEEE), Vol. 4, pp. 3108–3113.
7. Audoly S, Bellu G, D'Angiò L, Saccomani MP, Cobelli C (2001) Global identifiability of nonlinear models of biological systems. *IEEE transactions on bio-medical engineering* 48(1):55–65.
8. Meshkat N, Eisenberg M, Distefano JJ (2009) An algorithm for finding globally identifiable parameter combinations of nonlinear ODE models using Gröbner Bases. *Mathematical Biosciences* 222(2):61–72.
9. Raue A, et al. (2009) Structural and practical identifiability analysis of partially observed dynamical models by exploiting the profile likelihood. *Bioinformatics* 25(15):1923–9.
10. Eisenberg MC, Hayashi MAL (2014) Determining identifiable parameter combinations using subset profiling. *Mathematical Biosciences* 256:116–126.
11. Duintjer Tebbens RJ, et al. (2013) Characterizing poliovirus transmission and evolution: insights from modeling Experiences with wild and vaccine-related polioviruses. *Risk Analysis* 33(4):703–49.
12. Nathanson N, Kew OM (2010) From emergence to eradication: The epidemiology of poliomyelitis deconstructed. *American Journal of Epidemiology* 172(11):1213–1229.
13. Weather Atlas (2018) Monthly weather forecast and Climate: Be'er Sheva, Israel.
14. Yaari R, et al. (2016) Modeling the spread of polio in an IPV-vaccinated population: lessons learned from the 2013 silent outbreak in southern Israel. *BMC Medicine* 14(1):95.